

Bi-stability in a Mesoscopic Josephson Junction Array Resonator

P.R. Muppalla,^{1,2} O. Gargiulo,^{1,2} S.I. Mirzaei,^{1,2,3} B. Prasanna Venkatesh,^{1,4} M.L. Juan,¹ L. Grünhaupt,⁵ I.M. Pop,⁵ and G. Kirchmair^{1,2,*}

¹*Institute for Quantum Optics and Quantum Information, A-6020 Innsbruck, Austria*

²*Institute for Experimental Physics, University of Innsbruck, A-6020 Innsbruck, Austria*

³*Sharif University of Technology, Tehran, Iran*

⁴*Institute for Theoretical Physics, University of Innsbruck, A-6020 Innsbruck, Austria.*

⁵*Physikalisches Institut, Karlsruhe Institute of Technology, 76131 Karlsruhe, Germany*

(Dated: December 14, 2024)

We present an experimental investigation of the switching dynamics of a stochastic bistability in a 1000 Josephson junctions array resonator with a resonance frequency in the GHz range. As the device is in the regime where the anharmonicity is on the order of the linewidth, the bistability appears for a drive strength of only a few photons. We measure the dynamics of the bistability by continuously observing the jumps between the two metastable states, which occur with a rate ranging from a few Hz down to a few mHz. The switching rate strongly depends on the drive strength, pump strength and the temperature, following Kramer's law. The interplay between nonlinearity and coupling, in this little explored regime, could provide a new resource for nondemolition measurements, single photon switches or even elements for autonomous quantum error correction.

The non-linearity provided by atoms and Josephson junctions is a necessary ingredient to observe quantum mechanical effects in cavity quantum-electro-dynamics (QED) and circuit QED (cQED) systems. Strong nonlinearities, much larger than the linewidth of the transition, are required to realize qubits¹, implement quantum information protocols^{2,3} and realize textbook quantum optics experiments^{4,5}. Non-linearities much smaller than the linewidth of the transition are typically exploited for parametric processes⁶⁻⁸ like amplification or frequency conversion at the quantum level.

Besides quantum information applications, there has been a growing interest to exploit cavity QED for ultralow-power classical logic elements⁹⁻¹¹. This interest has been sparked by the ever growing all optical communication networks. Remarkably, a single photon transistor¹², reminiscent of an electronic transistor, has been implemented for the optical domain. In this device a single photon as a control can switch a large optical field. Realizing such devices has been a challenging endeavour as the required non-linearity is hard to realize, due to the weak interaction of optical light with atoms.

Much stronger light matter interactions can be achieved in the microwave regime using the cQED platform. In this context Josephson junction arrays (JJAs) have proven to be an ideal circuit element to build superconducting qubits with excellent coherence properties and unique tuning capabilities¹³⁻¹⁵. Similarly, JJAs have also been used to build quantum limited parametric amplifiers^{8,16-18}. Recently, the coherence properties of the self resonances of the array^{19,20}, as well as their self-Kerr and cross-Kerr coefficients have been measured²¹. The measured Kerr coefficient showed good agreement with a model based on a second order expansion of the Josephson potential²².

A regime of particular interest arises when the self-Kerr K_i and cross-Kerr K_{ij} nonlinear coefficients are on the order of the linewidth κ of the system. In this regime

the system will show a pronounced bi-stability^{23,24} at the single to few photon level. Bistability is a phenomenon which is relevant in many fields, ranging from chemistry²⁵ over biology^{26,27} to Josephson junction physics^{28,29}. Very recently, an optically levitated nanoparticle has been shown to exhibit a stochastic bistability³⁰ and Kramers turnover³¹.

In this Letter, we report on the realization of a JJA resonator with multiple modes and strong self-Kerr and cross-Kerr coefficients in the regime $K_i, K_{ij} \approx \kappa$. We investigate the bistability of one mode of the JJA and characterize the dependence of the switching rate on the drive strength, pump strength and temperature. The JJA consists of 10^3 cascaded Josephson junctions, with a small capacitance to ground C_0 , coupled to a 6 mm long microwave antenna and a shunt capacitance C_s , as shown in Fig. 1. The junctions are fabricated on a sapphire substrate using electron beam lithography and bridge-free double-angle evaporation³². An electron beam image of the junctions can be found in Fig. 1d. The junctions were designed to have a large ratio $E_J/E_C \approx 200$, in order to suppress coherent quantum phase slips (CQPS)^{33,34}. Here E_J is the Josephson junction energy and E_C is the charging energy. The parameters of the array were designed such that the fundamental resonance of the array combined with the shunt capacitance is around 1 GHz. The mode spacing for the first 10 modes is about 1.2 GHz and progressively becomes smaller for higher resonances^{20,21}.

The array is placed inside a copper waveguide with a 6 GHz cutoff, as shown in Fig. 1a. Due to the capacitive coupling of the array to the waveguide, we can characterize the sample by performing microwave transmission measurements using a vector network analyzer (VNA). Since the even modes of the JJA have a vanishing dipole moment, due to the symmetry of the electric field of the waveguide, only the odd modes of the array will couple to the waveguide and be visible

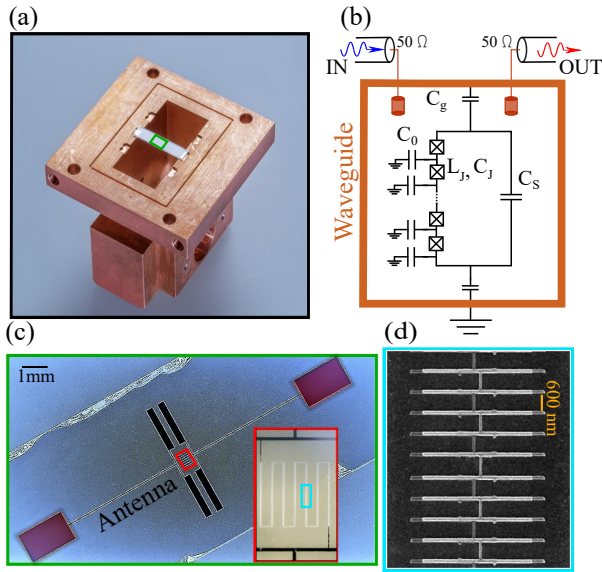


Figure 1. (a) Photograph of one half of a rectangular copper waveguide with a 6 GHz cutoff. A Josephson junction array with a microwave antenna is fabricated on a piece of sapphire and placed in the center of the waveguide (b) Schematic representation of an array of Josephson junctions inside a waveguide. C_0 is the capacitance of the islands to ground, C_S is the shunt capacitance for the array, C_J is the junction capacitance and C_g denotes the coupling capacitance of the antenna to the waveguide. L_J is the Josephson junction inductance. The input and output couplers to the waveguide are shown on the top left and top right of the schematic. (c) Optical image of the Josephson junction array coupled to a 6 mm long antenna and a shunt capacitance. The inset shows a zoom-in on the junction array. (d) Electron beam image (blue box in the inset) of ten of the 1000 Josephson junctions.

in transmission measurements. The waveguide with the sample is mounted on the mixing chamber stage (10 mK) of a cryogen free dilution refrigerator. The sample is enclosed in a double layer cryoperm shield inside a completely closed copper can. The stainless steel input lines are attenuated with 20 dB at 4 K and 30 dB at base temperature. They are filtered with a combination of a 12 GHz low pass and an Eccosorb filter. The output stage consists of a 12 GHz low pass filter, two 4-12 GHz isolators and a 4-8 GHz high electron mobility transistor amplifier. The effective measurement bandwidth for direct transmission measurements using a VNA is limited to about 4-9 GHz due to the cutoff of the waveguide and the combined bandwidth of other microwave components.

Within the accessible measurement bandwidth we can characterize three resonances by fitting their transmission data to a notch type response function³⁵. From these measurements we can extract the resonance frequencies (ω_i), the internal and the coupling quality factors (see supplementary material).

To observe the resonances of the modes outside the measurement bandwidth, we exploit the cross-Kerr interaction, which is induced by the junction non-

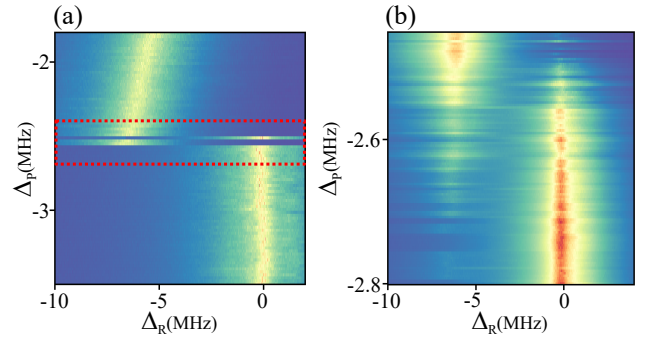


Figure 2. Two-tone measurement. (a) Shift Δ_R of the resonance frequency of the readout mode $\omega_R/2\pi = 7.105$ GHz upon application of a pump tone. The pump tone is detuned from the resonance $\omega_P/2\pi = 4.8156$ GHz of the 5th mode of the array by a detuning Δ_P and has a drive strength of $\bar{n}_P = 115$ photons. Due to the nonlinearity of the array, the resonance frequency of the readout mode is shifted when the pump tone matches mode five. (b) Zoom in on the bistable region of mode five. For a detuning of about $\Delta_P = -2.58(4)$ MHz two different resonance frequencies of the readout mode can be observed. The shifted and unshifted resonances correspond to 115 and 1 circulating photons in mode five, respectively.

linearity. The Hamiltonian for the array, up to second order, is given by

$$H = \sum_{i=1}^N (\omega_i a_i^\dagger a_i + \frac{K_i}{2} a_i^\dagger a_i a_i^\dagger a_i) + \sum_{\substack{i,j=1 \\ i \neq j}}^N K_{i,j} a_i^\dagger a_i a_j^\dagger a_j. \quad (1)$$

The Hamiltonian consists of a self-Kerr term which leads to a photon number $n_i = a_i^\dagger a_i$ dependent frequency shift K_i of mode i and a cross-Kerr interaction $K_{i,j}$, which leads to a frequency shift of mode i depending on the photon number in all other modes j .

In Fig.2 we show a two-tone spectroscopy where we sweep the frequency of a pump tone around mode five while weakly probing mode seven with the VNA. When the pump tone is resonant with mode five, we see a shift of the resonance frequency of mode seven. The measured frequency of mode five, using two-tone spectroscopy, matches the direct VNA measurement. We repeat this procedure, using mode seven as a readout, for frequencies between 900 MHz and 16 GHz. By comparing the measured frequencies of the entire array with the re-normalized mode frequencies calculated by diagonalizing the capacitance matrix (see supplementary material), we extract the device parameters $C_0 = 0.152$ fF, $C_J = 34$ fF, $L_J = 1.25$ nH, $C_S = 18$ fF with a confidence range of about 20 %. These parameters match well to the expected design values and room temperature resistance measurements of the junctions.

With these parameters we can calculate K_i and $K_{i,j}$ similar to Ref.²¹. The results are summarized in the supplementary material for modes five, seven and nine. Using these coefficients we can calibrate the photon

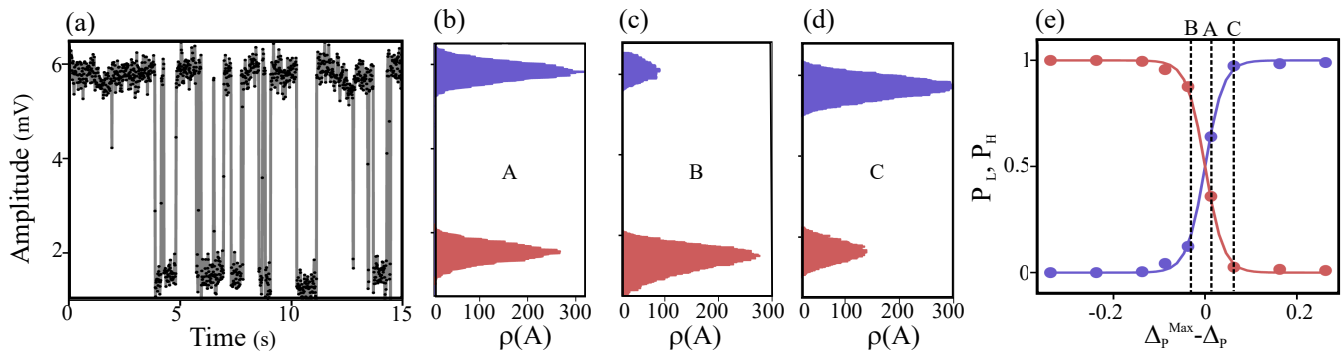


Figure 3. **(a)** Transitions from the low amplitude state to the high amplitude state for a pump strength of $\bar{n}_P = 9$ photons at a detuning of $\Delta_P \approx \Delta_P^{Max} = -0.54(1)$ MHz from mode five. The readout mode seven was driven with $\bar{n}_R = 0.5$ photons on resonance. The trace displayed here is a 15 s segment out of a total recorded time of 20000 s. **(b)** Histogram of the amplitude distribution $\rho(A)$ for the time trace displayed in **a**. **(c)** Histogram of the amplitude distribution $\rho(A)$ for a detuning of $\Delta_P = -0.59(1)$ MHz. **(d)** Histogram of the amplitude distribution $\rho(A)$ for a detuning of $\Delta_P = -0.49(1)$ MHz. **(e)**. Dependence of the normalized state population in the high and low photon state on Δ_P relative to the bistable point. The solid line is a fit to a sigmoid function.

number by measuring the resonance frequency shift as a function of the applied power (see supplementary material). The attenuation extracted from these Kerr measurements matches within 4% to the attenuation in the cryostat, determined by independent transmission measurements.

Upon closer inspection of the two-tone scan in Fig.2a one can observe a bistable region (see Fig.2b) for a detuning of $\Delta_P = -2.58$ MHz from the resonance frequency of mode five. Around this frequency, two different cross-Kerr shifts of mode seven can be observed. A shift of $\Delta_R = 7.32$ MHz corresponding to a photon number of about 115 photons in mode five and a shift of 133 kHz corresponding to about one photon. In the two-tone scan we observed that the residence time in either the high or low photon number states was exceeding ten seconds.

To precisely characterize the residence time, we implemented a readout scheme similar to the dispersive state detection of a superconducting qubit in a circuit QED architecture³⁶. We monitor mode seven continuously on resonance with a readout power of about half a photon such that we can not see an apparent shift or broadening of mode seven. When we pump mode five, we observe a change in the transmitted readout signal corresponding to jumps between the high and the low amplitude states. For each datapoint we average 500 measurements each lasting $19.9 \mu\text{s}$ to get a good signal to noise ratio. In addition, the analog to digital converter needs another 5 ms to transfer the data. Thus, it takes about 15 ms to acquire one datapoint.

In Fig.3a we show a typical time trace for a measurement time of 15 s and a photon number of about 9 photons in mode five. One can clearly observe two distinct amplitudes in transmission corresponding to two distinct photon numbers in mode five. The transient time between these two states is much faster

than the data acquisition rate and will be on the order of $1/\kappa_5$, which means between $1 - 100 \mu\text{s}$ depending on the drive strength of mode five. A histogram of the data shows a well separated bi-modal distribution for the two amplitude states. Furthermore, we extract the residence times in the high amplitude state from one up-transition to the next down transition and plot the results as a histogram (see supplementary material). The exponential dependence of the residence time indicates that the transitions are random and follow a Poisson statistics. From an exponential fit to the data we extract a mean residence time in the high state of $T_{up} = 14.4$ s. When we sweep the detuning of the pump frequency Δ_P across the bistable point we see a change of the relative height of the peaks in the amplitude distribution Fig.3b-e. There is a Δ_P^{Max} for a given drive strength where the heights of the peaks are equal as shown for example in Fig.3b.

We repeat the switching rate measurements for a total of ten different pump powers ranging from 2.6 to 115 photons in mode five. In Fig.4b we plot the maximally achieved switching rate and the corresponding drive detuning Δ_P^{Max} versus photon number. The first time we observe switching is for a drive power of 2.6 photons at a detuning of -169 kHz from the low power resonance. This detuning matches well to the prediction³⁷ of $\Delta_P = \sqrt{3}/2 \kappa_5 = 160$ kHz with $\kappa_5 = 187$ kHz.

Typically, stochastic switching in a bistable system is described by Kramers law³⁸. There, the switching rate is determined by the potential landscape and the fluctuations. For a symmetric potential it is given by $\Gamma_{Max} = \Gamma_0 \exp(-E_b/k_bT)$, where E_b is the barrier height between the two stable solutions and the prefactor Γ_0 which depends on the relative strength of the dissipation and the potential³⁸. In our case, the activation of the switching between the two stable solutions likely originates from the dispersive shift of the resonator

frequency due to photon number fluctuations in the readout mode and thermal fluctuations of the photon number in all modes.

In our case, the potential landscape is created by the interplay between the drive, the self-Kerr effect and the damping of the mode. An intuitive choice for this potential^{23,24} is provided by integrating the equation for the photon number in the steady state of a damped Kerr oscillator³⁹. From this model we extract the scaling of E_b ⁴⁰ and Γ_0 for the maximum switching rate as a function of the pump photon number \bar{n}_P . We use this scaling in a fit function (see Fig. 4b) with two parameters to match our data (see supplementary material). We also add a Γ_{res} to take into account the finite switching rate for high drive powers. This finite rate could be limited by phase slips on the junctions of the array, which we estimated to be in the range of a few mHz.

Additionally, we observe a change of the switching rate with respect to Δ_P following a lorentzian curve. The point of maximum switching rate Δ_P^{Max} also corresponds to a symmetric amplitude distribution. In Fig.4a one can see the change of the switching rate with respect to Δ_P for three different drive powers. The switching rate Γ is the inverse of the average time between two transitions from the low to the high power state. The width of this lorentzian is about 72 kHz and the center shifts with increasing photon number in the pump. From our model we can also extract the shift of Δ_P^{Max} with \bar{n}_P which agrees well with the experiment as shown in Fig. 4b. The deviation at high photon numbers can be explained by higher order Kerr effects which are not taken into account in the model.

To better identify the origin of the switching we varied the power in the readout tone. The measured results are plotted in Fig.4c for a constant pump power of 6 photons. We can observe two effects for an increasing photon number in the readout mode: I) due to the cross-Kerr effect the bistable point moves to lower frequencies. II) in contrast to lowering the switching rate with the pump photon number, the readout photon number increases the switching rate. For a readout of 2.5 photons we see an increase in the switching rate by about a factor of three. This can be understood as a form of measurement induced dephasing. As the photon number in the readout resonator fluctuates, the position of the bistable point moves in frequency due to the cross-Kerr effect. This moves the drive in and out of the bistable region into the regime where either the low or the high power state are more likely as the cross-Kerr is on the order of the linewidth. This photon number fluctuation happens at a rate $\kappa_7 = 7.5$ MHz and is thus much faster than our acquisition time. For drive powers higher than 2.5 photons, the switching becomes much faster and we cannot observe it any more due to the limited bandwidth and signal to noise. Also notice, changing \bar{n}_R by one photon for a constant Δ_P we can switch the state of mode five from the low to the high photon number occupation.

To study the influence of thermal noise on the

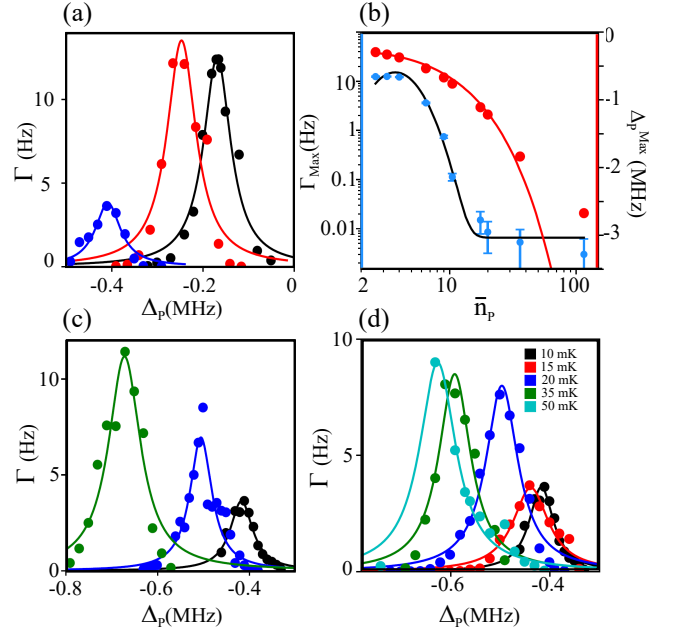


Figure 4. (a) Switching rate Γ for a pump detuning Δ_P for three different pump strength: \bullet $\bar{n}_P = 2.6$ photons, \bullet $\bar{n}_P = 4$ photons, \bullet $\bar{n}_P = 6$ photons. The solid lines are lorentzian fits to the data. (b) Extracted maximum switching rate Γ_{Max} and corresponding pump detuning Δ_{Max} as a function of the pump strength \bar{n}_P . The black line is a exponential fit to the data with an additional constant (see text). (c) Γ measured for a constant pump strength of $\bar{n}_P = 6$ photons while varying the readout strength: \bullet $\bar{n}_R = 0.5$ photons, \bullet $\bar{n}_R = 1.5$ photons, \bullet $\bar{n}_R = 2.5$ photons. (d) Γ measured for different cryostat base temperatures with $\bar{n}_P = 6$. In (a), (b) and (d) $\bar{n}_R = 0.5$.

switching rate, we increased the cryostat base plate temperature from 10 mK to 50 mK. The pump power was kept constant at 6 photons while the readout power was at 0.5 photons. Similar to the increase in readout power we can observe the same two effects in the maximum switching rate, which are again due to the cross-Kerr interactions of mode five with all other modes. Increasing the temperature increases the average thermal population as well as the fluctuations of the photon number in all of the modes of the array, most notably for the lower frequency modes. The observed shift can be explained, by an increase in the device temperature up to about 100-130 mK depending on the initial temperature. We can get an upper bound for the device temperature at the base temperature of the fridge, if we assume that the linewidth broadening we observe for mode five (see supplementary material) is due to the thermal population in the other modes of the array. This broadening can be explained by a temperature of the array of ≈ 50 mK being above the base temperature of the fridge, which is consistent with other cQED experiments^{41,42}.

In conclusion, we have measured a stochastic bistability in a 1000 Josephson junction array which

appears at a drive strength of only a few photons. This switching at low power is achieved by engineering the Kerr interaction strength to be comparable to the linewidth. We have seen an exponential decrease of the maximal switching rate for increasing drive strength as expected from Kramers law. For an increase in readout strength or temperature, the switching rate increases, likely due to photon induced dephasing through cross-Kerr interactions.

This proof of principle device demonstrates that it is possible for a single microwave photon in the readout mode to switch the photon occupation number by two orders of magnitude in the pump mode. As such it is a promising system to implement novel types of nondemolition measurements⁴³, single photon microwave

transistors^{44,45}, single photon microwave switches⁴⁶, Flip-Flop memories⁴⁷ or even elements for autonomous quantum error correction¹⁰.

We gratefully acknowledge fruitful discussions with Christian Kraglund Andersen, Alexandre Blais, Archana Kamal, Zlatko Mineev, Michel Devoret, Peter Talkner, Michael Marthaler and Linghzen Guo. We thank Luigi Frunzio for help with the fabrication of a first generation junction array resonator. IMP and LG acknowledge funding provided by the Alexander von Humboldt Foundation in the framework of the Sofja Kovalevskaja Award endowed by the German Federal Ministry of Education and Research. Facilities use was supported by the KIT Nanostructure Service Laboratory (NSL). We also thank Christian Schneider valuable comments on the manuscript.

-
- * gerhard.kirchmair@uibk.ac.at
- ¹ H. Paik, D. I. Schuster, L. S. Bishop, G. Kirchmair, G. Catelani, A. P. Sears, B. R. Johnson, M. J. Reagor, L. Frunzio, L. I. Glazman, S. M. Girvin, M. H. Devoret, and R. J. Schoelkopf, *Physical Review Letters* **107**, 240501 (2011).
 - ² J. Kelly, R. Barends, A. G. Fowler, A. Megrant, E. Jeffrey, T. C. White, D. Sank, J. Y. Mutus, B. Campbell, Y. Chen, Z. Chen, B. Chiaro, A. Dunsworth, I.-C. Hoi, C. Neill, P. J. J. O'Malley, C. Quintana, P. Roushan, A. Vainsencher, J. Wenner, A. N. Cleland, and J. M. Martinis, *Nature* **519**, 66 (2015).
 - ³ A. D. Córcoles, E. Magesan, S. J. Srinivasan, A. W. Cross, M. Steffen, J. M. Gambetta, and J. M. Chow, *Nature Communications* **6**, 6979 (2015).
 - ⁴ L. Sun, A. Petrenko, Z. Leghtas, B. Vlastakis, G. Kirchmair, K. M. Sliwa, A. Narla, M. Hatridge, S. Shankar, J. Blumoff, L. Frunzio, M. Mirrahimi, M. H. Devoret, and R. J. Schoelkopf, *Nature* **511**, 444 (2014).
 - ⁵ C. Wang, Y. Y. Gao, P. Reinhold, R. W. Heeres, N. Ofek, K. Chou, C. Axline, M. Reagor, J. Blumoff, K. M. Sliwa, L. Frunzio, S. M. Girvin, L. Jiang, M. Mirrahimi, M. H. Devoret, and R. J. Schoelkopf, *Science* **352**, 1087 (2016).
 - ⁶ I. Siddiqi, R. Vijay, F. Pierre, C. M. Wilson, M. Metcalfe, C. Rigetti, L. Frunzio, and M. H. Devoret, *Physical Review Letters* **93**, 207002 (2004).
 - ⁷ N. Bergeal, R. Vijay, V. E. Manucharyan, I. Siddiqi, R. J. Schoelkopf, S. M. Girvin, and M. H. Devoret, *Nature Physics* **6**, 296 (2010).
 - ⁸ A. Roy and M. Devoret, *Comptes Rendus Physique Quantum microwaves / Micro-ondes quantiques*, **17**, 740 (2016).
 - ⁹ H. Mabuchi, *Physical Review A* **80**, 045802 (2009).
 - ¹⁰ J. Kerckhoff, H. I. Nurdin, D. S. Pavlichin, and H. Mabuchi, *Physical Review Letters* **105**, 040502 (2010).
 - ¹¹ R. Bose, D. Sridharan, H. Kim, G. S. Solomon, and E. Waks, *Physical Review Letters* **108**, 227402 (2012).
 - ¹² W. Chen, K. M. Beck, R. Bücker, M. Gullans, M. D. Lukin, H. Tanji-Suzuki, and V. Vuletić, *Science* **341**, 768 (2013).
 - ¹³ V. E. Manucharyan, J. Koch, L. I. Glazman, and M. H. Devoret, *Science* **326**, 113 (2009).
 - ¹⁴ I. M. Pop, K. Geerlings, G. Catelani, R. J. Schoelkopf, L. I. Glazman, and M. H. Devoret, *Nature* **508**, 369 (2014).
 - ¹⁵ M. Bell, W. Zhang, L. Ioffe, and M. Gershenson, *Physical Review Letters* **116**, 107002 (2016).
 - ¹⁶ C. Macklin, K. O'Brien, D. Hover, M. E. Schwartz, V. Bolkhovskoy, X. Zhang, W. D. Oliver, and I. Siddiqi, *Science* **350**, 307 (2015).
 - ¹⁷ M. A. Castellanos-Beltran, K. D. Irwin, G. C. Hilton, L. R. Vale, and K. W. Lehnert, *Nature Physics* **4**, 929 (2008).
 - ¹⁸ C. Eichler and A. Wallraff, *EPJ Quantum Technology* **1**, 2 (2014).
 - ¹⁹ C. Hutter, E. A. Tholén, K. Stannigel, J. Lidmar, and D. B. Haviland, *Physical Review B* **83**, 014511 (2011).
 - ²⁰ N. A. Masluk, I. M. Pop, A. Kamal, Z. K. Mineev, and M. H. Devoret, *Physical Review Letters* **109**, 137002 (2012).
 - ²¹ T. Weißl, B. Küng, E. Dumur, A. K. Feofanov, I. Matei, C. Naud, O. Buisson, F. W. J. Hekking, and W. Guichard, *Physical Review B* **92**, 104508 (2015).
 - ²² J. Bourassa, F. Beaudoin, J. M. Gambetta, and A. Blais, *Physical Review A* **86**, 013814 (2012).
 - ²³ M. Marthaler and M. I. Dykman, *Physical Review A* **73**, 042108 (2006).
 - ²⁴ L. Guo, Z. Zheng, X.-Q. Li, and Y. Yan, *Physical Review E* **84**, 011144 (2011).
 - ²⁵ P. L. García-Müller, F. Borondo, R. Hernandez, and R. M. Benito, *Physical Review Letters* **101**, 178302 (2008).
 - ²⁶ M. D. McDonnell and L. M. Ward, *Nature Reviews Neuroscience* **12**, 415 (2011).
 - ²⁷ V. M. Eguíluz, M. Ospeck, Y. Choe, A. J. Hudspeth, and M. O. Magnasco, *Physical Review Letters* **84**, 5232 (2000).
 - ²⁸ P. Silvestrini, S. Pagano, R. Cristiano, O. Liengme, and K. E. Gray, *Physical Review Letters* **60**, 844 (1988).
 - ²⁹ E. Turlot, D. Esteve, C. Urbina, J. M. Martinis, M. H. Devoret, S. Linkwitz, and H. Grabert, *Physical Review Letters* **62**, 1788 (1989).
 - ³⁰ F. Ricci, R. A. Rica, M. Spasenović, J. Gieseler, L. Rondin, L. Novotny, and R. Quidant, *Nature Communications* **8**, 15141 (2017).
 - ³¹ L. Rondin, J. Gieseler, F. Ricci, R. Quidant, C. Dellago, and L. Novotny, (2017), arXiv:1703.07699.
 - ³² F. Lecocq, I. M. Pop, Z. Peng, I. Matei, T. Crozes, T. Fournier, C. Naud, W. Guichard, and O. Buisson,

- Nanotechnology **22**, 315302 (2011).
- ³³ I. M. Pop, I. Protopopov, F. Lecocq, Z. Peng, B. Pannetier, O. Buisson, and W. Guichard, *Nature Physics* **6**, 589 (2010).
- ³⁴ V. E. Manucharyan, N. A. Masluk, A. Kamal, J. Koch, L. I. Glazman, and M. H. Devoret, *Physical Review B* **85**, 024521 (2012).
- ³⁵ S. Probst, F. B. Song, P. A. Bushev, A. V. Ustinov, and M. Weides, *Review of Scientific Instruments* **86**, 024706 (2015).
- ³⁶ A. Blais, R.-S. Huang, A. Wallraff, S. M. Girvin, and R. J. Schoelkopf, *Physical Review A* **69**, 062320 (2004).
- ³⁷ F. R. Ong, M. Boissonneault, F. Mallet, A. Palacios-Laloy, A. Dewes, A. C. Doherty, A. Blais, P. Bertet, D. Vion, and D. Esteve, *Physical Review Letters* **106**, 167002 (2011).
- ³⁸ P. Hänggi, P. Talkner, and M. Borkovec, *Reviews of Modern Physics* **62**, 251 (1990).
- ³⁹ G. P. Agrawal and H. J. Carmichael, *Physical Review A* **19**, 2074 (1979).
- ⁴⁰ D. G. Luchinsky, R. Mannella, P. V. E. McClintock, M. I. Dykman, and V. N. Smelyanskiy, *Journal of Physics A: Mathematical and General* **32**, L321 (1999).
- ⁴¹ K. Geerlings, Z. Leghtas, I. M. Pop, S. Shankar, L. Frunzio, R. J. Schoelkopf, M. Mirrahimi, and M. H. Devoret, *Physical Review Letters* **110**, 120501 (2013).
- ⁴² X. Jin, A. Kamal, A. Sears, T. Gudmundsen, D. Hover, J. Miloshi, R. Slattery, F. Yan, J. Yoder, T. Orlando, S. Gustavsson, and W. Oliver, *Physical Review Letters* **114**, 240501 (2015).
- ⁴³ S. Kumar and D. P. DiVincenzo, *Physical Review B* **82**, 014512 (2010).
- ⁴⁴ L. Neumeier, M. Leib, and M. J. Hartmann, *Physical Review Letters* **111**, 063601 (2013).
- ⁴⁵ M. T. Manzoni, F. Reiter, J. M. Taylor, and A. S. Sørensen, *Physical Review B* **89**, 180502 (2014).
- ⁴⁶ J.-Q. Liao, J.-F. Huang, Y.-x. Liu, L.-M. Kuang, and C. P. Sun, *Physical Review A* **80**, 014301 (2009).
- ⁴⁷ C. K. Andersen and K. Mølmer, *Physical Review Applied* **3**, 024002 (2015).